Appl Phys A (2010) 99: 29–37
DOI 10.1007/s00339-010-5571-x

Applied Physics A
Materials Science & Processing

A theoretical study of hydrogen adsorption on Li, Be, Na, and Mg atoms attached to aromatic hydrocarbons

Shigeru Ishikawa · Tokio Yamabe

Received: 30 April 2009 / Accepted: 22 January 2010 / Published online: 6 February 2010

Abstract The binding energy of a hydrogen molecule on metal atoms (Li, Be, Na, and Mg) attached to aromatic hydrocarbon molecules (benzene and anthracene) was calculated using an ab initio molecular orbital method at the MP2(FC)/cc-pVTZ level with basis set superposition error (BSSE) correction. The energy tended to become more negative as the metal atom had a more positive charge and a smaller radius. The energies of $Li_2C_6H_6$-H_2, $Li_2C_{14}H_{10}$-H_2, $Na_2C_{14}H_{10}$-H_2, and $MgC_{14}H_{10}$-H_2 were -2.7 to -2.2, -4.0 to -3.1, -2.8 to -0.3, and -1.3 kcal/mol, respectively. Most of these energies were more negative than those on the hydrocarbons without metal atoms (ca. -1 kcal/mol). Analyzing the Lennard–Jones type potential with the parameters determined by the MP2 calculations, it was found that these energies mainly consisted of the induction force caused by the positive charge of the metal atom and the dispersion force from the nearest C_6-ring. The energy of $BeC_{14}H_{10}$-H_2 was more negative (-8.6 kcal/mol) than of the other complexes. The hydrogen molecule in this complex had a comparatively longer H–H distance and a more positive H_2 charge than the others. These data suggest that the hydrogen adsorption on this complex involves a charge transfer process in addition to physisorption interactions. The hydrogen binding energies in some $Li_2C_{14}H_{10}$-H_2 systems (~ -4.0 kcal/mol) and $BeC_{14}H_{10}$-H_2 are promising to operate hydrogen storage/release at ambient temperature with moderate pressure.

S. Ishikawa (✉)
Department of Chemistry, Faculty of Science, Tokai University, 1117 Kitakaname, Hiratsuka 259-1292, Japan
e-mail: sisikawa@keyaki.cc.u-tokai.ac.jp
Fax: +81-463502094

T. Yamabe
Nagasaki Institute of Applied Science, 536 Aba-machi, Nagasaki 851-0193, Japan

1 Introduction

Hydrogen fuel cells have attracted much attention as a new power source to replace internal combustion engines that use fossil fuels. To put fuel-cell loaded vehicles to a practical use, hydrogen storage densities should be more than 6 wt%, as proposed by the US Department of Energy (DOE) [1]. To achieve this target, many hydrogen storage materials, such as metal hydrides, porous adsorbents (carbons, metal-organic frameworks, polymers, and zeolites), and hydrogen clathrates, have been investigated [2]. Among the porous adsorbents, activated carbons and carbon nanostructures have been extensively investigated because their small pores give them large surface areas and enhance the interactions between hydrogen molecules and their surfaces [2]. Early experiments on carbon nanotubes showed a large amount of hydrogen storage, exceeding the DOE target density at ambient temperature [3]; however, it was immediately pointed out that impurities such as Ti-alloy particles produced in preparing the sample or water in hydrogen gas apparently increased the hydrogen storage [4, 5]. At present, the maximum hydrogen storage is found to be 4 wt% at 77 K and less than 1 wt% at ambient temperature [6–10].

The interaction between hydrogen and carbon materials is intrinsically weak. For example, scattering experiments of a hydrogen molecule on a (0001) graphite surface showed that the hydrogen binding energy on the graphite surface was about -1 kcal/mol [11, 12]. Monte Carlo simulations of the hydrogen adsorption on several nanocarbons showed that none of these satisfied the DOE target density at moderate conditions [13]. It is thought that carbon materials cannot

sufficiently adsorb hydrogen without cryogenic temperature and high pressure.

The attractive interaction between a hydrogen molecule and carbon materials is dominated by the dispersion force. Another kind of force is necessary to strengthen the attraction. A promising method of providing an attractive force is to dope the carbon materials with alkali metal atoms [13]. Doped alkali metal atoms in carbon materials have positive charges, which cause an induction force by which they can adsorb hydrogen molecules. These metal atoms may enhance the dispersion force by changing polarizability of the carbon atoms. On the other hand, it was reported that the amount of hydrogen storage on Li-doped nanotubes using pure hydrogen gas did not exceed the target density [5]. It seems that Li doping does not enhance the amount of hydrogen storage; however, the adsorption mechanism has not yet been resolved in this system, and the role of Li atoms remains unknown.

In this connection, we investigated the interaction between a hydrogen molecule and a metal atom doped in carbon materials, from a microscopic point of view, by using an ab initio molecular orbital method. Alkali metal atoms examined in this study were Li and Na. Group 2 metal atoms, Be and Mg, were also examined because they can have more positive charges than alkali metal atoms. These atoms were attached to the benzene or anthracene molecules, which were used to represent the constituent units of carbon materials.

The employed model molecules are rather small and their hydrogen binding energies may deviate from those of real carbon materials. However, the results of ab initio calculations of small molecules are often adopted in deriving the parameters of the empirical potentials used in molecular dynamics simulations of large systems [14, 15]. Physisorption and diffusion of hydrogen atoms on graphite surface were reported using the potential determined by the MP2 calculation of the hydrogen–coronene system [14]. Liquefaction of H_2 molecules on carbon nanotubes was studied [15] using the ReaxFF potential [16] which was designed so as to reproduce the results of the quantum chemical calculations of small hydrocarbon molecules. These results show that the intermolecular interaction energies obtained in small molecular systems can be adopted for those in large systems if the molecular systems are properly chosen.

This paper is organized as follows. First, the hydrogen binding energy on hydrocarbons without metal atoms is shown by changing the orientation of a hydrogen molecule. Second, the binding energies of the metal atoms on hydrocarbons and their charges and bonding characters are reported. Finally, hydrogen binding energies on the metal atoms attached to the hydrocarbons are shown and the adsorption mechanism is analyzed by decomposing the binding energy into induction and dispersion energies using Lennard–Jones type potentials.

2 Method of calculation

Ab initio molecular orbital calculations were performed using Gaussian03 [17]. Molecular structures were optimized based on the second-order Møller–Plesset (MP2) theory [18] with frozen core (FC) approximation using the cc-pVTZ basis set [19]. The optimization thresholds were reduced using the program's "tight" option. The basis set superposition error (BSSE) for the hydrogen adsorption energy was estimated by the counterpoise (CP) method [20, 21]. Atomic charges were calculated by the natural population analysis (NPA) [22] using the MP2 density obtained by the generalized density method [23]. The contribution of the zero-point vibrational energy (ZPE) to the total energy was not evaluated in this study.

3 Results and discussion

3.1 Hydrogen adsorption on aromatic hydrocarbons

The hydrogen adsorption on aromatic hydrocarbons (benzene and anthracene) was examined by setting the orientation of a hydrogen molecule parallel or vertical to the molecular plane of the hydrocarbons. The nuclear framework of the H_2–hydrocarbon complex was fixed at the C_{2v} symmetry during the optimization. The optimized structures are shown in Fig. 1. The binding energy of a hydrogen molecule (ΔE_{H2}) is shown in Table 1 with the distance between the center of mass of the hydrogen molecule and that of the C_6-ring ($R_{C_6\text{–}H_2}$) for each complex. A negative sign for the binding energy means that the adsorption process is exothermic. By comparing structures having the same H_2 orientation, it is observed that the H_2–anthracene complex has more negative binding energy and a shorter C_6–H_2 distance than the H_2–benzene complex. The vertical orientation gives more negative binding energy than the parallel one for both hydrocarbons but the differences between the H_2–anthracene complexes are small. These results are consistent with the preceding theoretical studies using different methods [24, 25].

It was reported that the hydrogen binding energy on the (0001) graphite surface was −1.19 kcal/mol (−0.96 kcal/mol with the ZPE correction), and the equilibrium distance from the surface was 2.87 Å [11, 12]. The calculated values of the binding energies (−1.0 to −0.9 kcal/mol) and the equilibrium C_6–H_2 distances (2.88 to 3.00 Å) of the H_2–anthracene complexes are close to these experimental results. It has been reported that the magnitude of the hydrogen binding energy did not depend strongly on the size of the aromatic hydrocarbon [24].

The MP2 method sometimes overestimates the intermolecular interaction. For example, the MP2 calculation of

Table 1 Binding energy of a hydrogen molecule adsorbed on aromatic hydrocarbon molecules (ΔE_{H_2}), the distance between the center of mass of the H_2 molecule and that of the C_6-ring ($R_{H_2-C_6}$), and Lennard–Jones parameters (A and B). The energy without CP correction is shown in parentheses

	ΔE_{H_2}/kcal mol^{-1}	$R_{H_2-C_6}$/Å	$A/10^5$ kcal mol^{-1} Å^{12}	$B/10^3$ kcal mol^{-1} Å^6
C_6H_6-H_2				
1	−0.5(−0.7)	3.01	2.82	0.76
2	−0.5(−0.7)	3.01	2.81	0.76
3	−0.9(−1.1)	3.07	6.16	1.47
Average			3.93	1.00
$C_{14}H_{10}$-H_2				
4	−0.9(−1.1)	2.88	2.80	0.99
5	−0.9(−1.2)	2.96	4.01	1.20
6	−1.0(−1.4)	3.00	5.58	1.53
Average			4.13	1.24

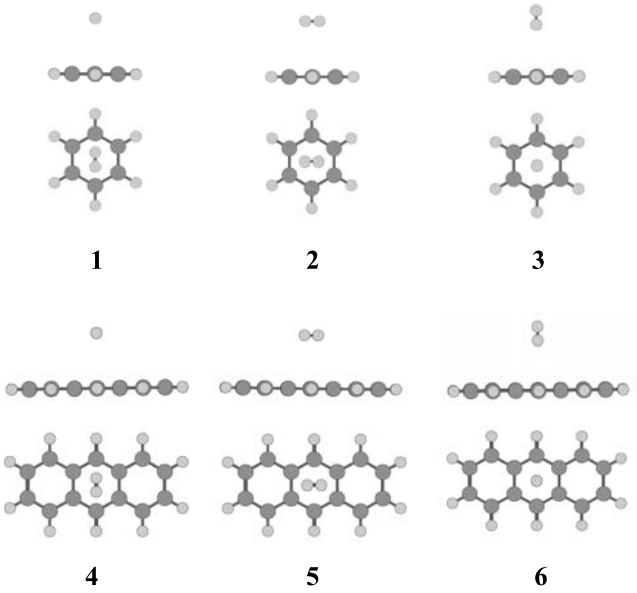

Fig. 1 Optimized structures of aromatic hydrocarbon molecules adsorbing a hydrogen molecule. The symmetry of the system is restricted to C_{2v}

a benzene dimer gives a larger binding energy than the experiment. Two experimental values were reported for this system, $D_0 = 1.6 \pm 0.2$ [26] and 2.4 ± 0.4 kcal mol^{-1} [27]. Three configurations (sandwich, T-shaped, and parallel displaced) have been studied by using several methods [28–30]. The MP2 calculation with aug-ccpVTZ basis set gave $D_e =$ 3.26, 3.46, and 4.67 kcal mol^{-1} [28], while the CCSD(T) calculation taking complete basis set (CBS) limit gave 1.81, 2.74, and 2.78 kcal mol^{-1} [28] for the sandwich, T-shaped, and parallel displaced, respectively. The MP2 binding energy is particularly large in the sandwich and parallel displaced configurations where the dispersion force dominates the intermolecular interaction, while it is not so large in the T-shaped configuration where electrostatic interactions are important [30]. The error of the MP2 method is mainly due to the overestimation of the π–π interaction between benzene molecules.

In our case, the binding energies of a H_2 molecule on aromatic hydrocarbons calculated by the MP2/cc-pVTZ level are 0.9–1.0 kcal mol^{-1}, which are about 80% of the binding energy on the graphite surface. The CBS limit will increase the MP2 binding energy, however, its magnitude will be ∼0.4 kcal/mol expecting from the results of the benzene dimer [28–30] or other calculations [31]. We did not observe extremely large overestimations or underestimations for the H_2–hydrocarbon systems.

The molecular interaction potential between nonpolar molecules separated by a distance R is often described by the Lennard–Jones potential:

$$U_{L-J}(R) = \frac{A}{R^{12}} - \frac{B}{R^6}. \quad (1)$$

The parameters A and B for the H_2–hydrocarbon complexes derived from ΔE_{H2} and $R_{C_6-H_2}$ are shown in Table 1. The averages of these parameters (A_{av} and B_{av}) will be used to analyze the interaction between a hydrogen molecule and the C_6-ring of aromatic hydrocarbons having metal atoms.

3.2 Binding energies and charges of Li, Na, Be, and Mg atoms attached to aromatic hydrocarbons

Li, Na, Be, and Mg atoms were attached to aromatic hydrocarbons (benzene and anthracene) and their binding energies, atomic charges, and bonding properties were investigated. One or two metal atoms were attached to the hydrocarbon molecule to achieve a closed electron configuration. Calculated complexes were $Li_2C_6H_6$ (**7** and **8**), $Li_2C_{14}H_{10}$ (**9** and **10**), $Na_2C_{14}H_{10}$ (**11** and **12**), $BeC_{14}H_{10}$ (**13**), and $MgC_{14}H_{10}$ (**14**).

Figure 2 shows their optimized structures. Before MP2 optimization calculations, structures **7**–**14** were optimized at B3LYP/6-31G** level and confirmed that each structure was located on the minimum of the potential surface by the

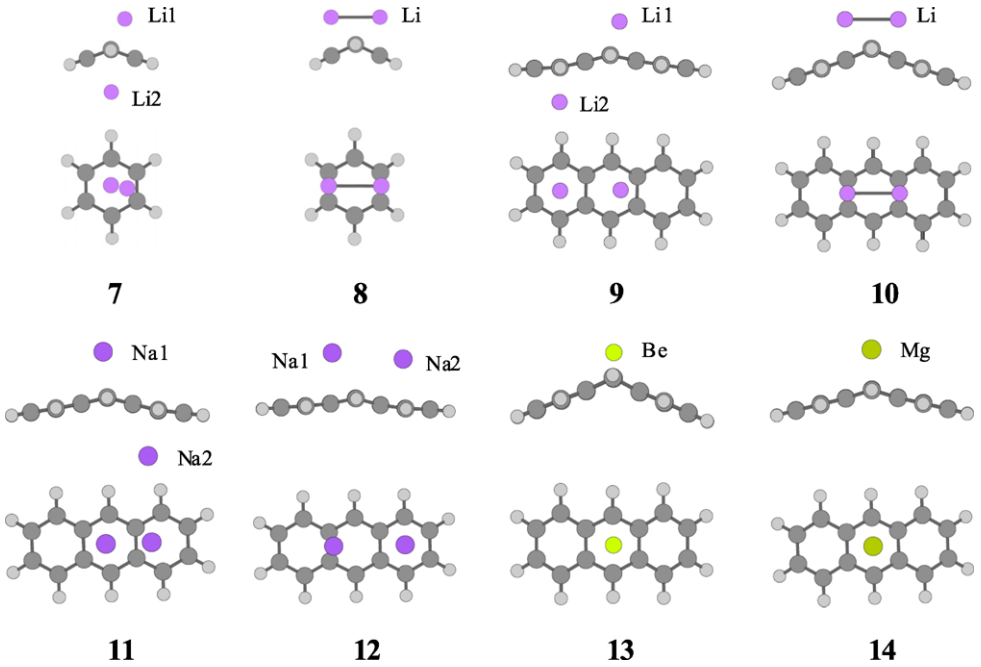

Fig. 2 Optimized structures of aromatic hydrocarbon molecules with a metal atom attached: $Li_2C_6H_6$ (**7** and **8**), $Li_2C_{14}H_{10}$ (**9** and **10**), $Na_2C_{14}H_{10}$ (**11** and **12**), $BeC_{14}H_{10}$ (**13**), and $MgC_{14}H_{10}$ (**14**)

Table 2 Binding energy per metal atom attached to aromatic hydrocarbons (ΔE_M), the NPA charge of the metal (q_M), and the distance between the metal and the carbon atom (R_{M-C})

	ΔE_M/kcal mol^{-1}	q_M	R_{M-C}/Å
$Li_2C_6H_6$			
7	−13.2	0.736(Li1)0.728(Li2)	2.16(Li1) 2.19(Li2)
8	−18.0	0.732	2.06
$Li_2C_{14}H_{10}$			
9	−30.1	0.859(Li1)0.910(Li2)	2.18(Li1) 2.15(Li2)
10	−29.6	0.778	2.07
$Na_2C_{14}H_{10}$			
11	−14.0	0.886(Na1)0.711(Na2)	2.58(Na1)2.62(Na2)
12	−14.4	0.572(Na1)0.591(Na2)	2.56(Na1)2.59(Na2)
$BeC_{14}H_{10}$			
13	−27.6	1.301	1.75
$MgC_{14}H_{10}$			
14	−1.8	0.818	2.33

vibrational analysis. The symmetries of the structures were C_1 (**7**), C_{2v} (**8**, **10**, **13**, **14**), and C_s (**9**, **11**, **12**). For $Li_2C_{14}H_{10}$ and $Na_2C_{14}H_{10}$, several structures are examined. Structures **9** (**10**) is the most stable structure among $Li_2C_{14}H_{10}$ molecules having two Li atoms on the opposite sides (on the same side). Structures **11** (**12**) is also the most stable structure among $Na_2C_{14}H_{10}$ molecules having two Na atoms on the opposite sides (on the same side). For $BeC_{14}H_{10}$ and $MgC_{14}H_{10}$, structures other than **13** and **14** were not examined. The MP2 optimization was done at the symmetry obtained in the previous calculation.

Carbon skeletons in Fig. 2 are largely deformed from the original ones. These deformations help hydrocarbon molecules to accommodate metal atoms [32]. Alkali metal atoms are attached either on the same side (**8**, **10**, and **12**) or on the opposite sides (**7**, **9**, and **11**) of the molecular plane. Two Li atoms in **8** or **10** form a Li dimer. The Li–Li distance of each dimer (2.45 Å for **8** and 2.52 Å for **10**) is shorter than that of the isolated Li_2 molecule (2.75 Å). The mechanism of Li dimerization on aromatic hydrocarbons was elucidated in terms of the orbital interaction between a Li_2 molecule and the C_6-ring of the hydrocarbon [32].

The binding energy per metal atom and the NPA charge of the metal atom are shown in Table 2. The Li–anthracene complexes show more negative Li binding energies (∼−30 kcal/mol) and more positive Li atomic charges (0.78 to 0.91) than the Li–benzene complexes (−18 to −13 kcal/mol and 0.73 to 0.74). A plausible reason for

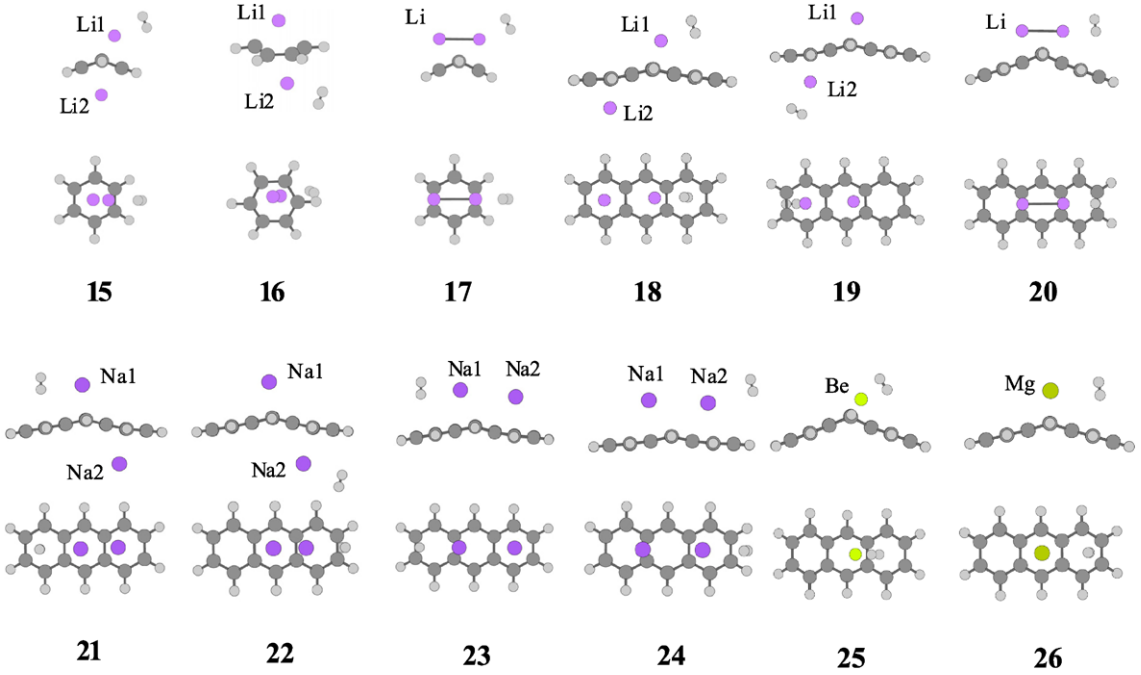

Fig. 3 Optimized structures of aromatic hydrocarbon molecules with a metal atom attached adsorbing a hydrogen molecule: $Li_2C_6H_6$-H_2 (**15**–**17**), $Li_2C_{14}H_{10}$-H_2 (**18**–**20**), $Na_2C_{14}H_{10}$-H_2 (**21**–**24**), $BeC_{14}H_{10}$-H_2 (**25**), and $MgC_{14}H_{10}$-H_2 (**26**)

this difference is that the anthracene molecule has greater electron affinity than the benzene molecule. Comparing the second-row atom with the third one in the same group, it is found that the former shows a more negative binding energy and tends to become more positive than the latter. The Li binding energies of structures **9** and **10** (∼−30 kcal/mol) are more negative than the Na binding energies of **11** and **12** (∼−14 kcal/mol). The Li atomic charges of **9** and **10** lie in the more positive range (0.78 to 0.91) than the Na atomic charges of **11** and **12** (0.57 to 0.89). The binding energy of the Be atom in **13** is more negative (∼−28 kcal/mol) than that of the Mg atom in **14** (∼−2 kcal/mol), and the Be atomic charge (1.3) is more positive than the Mg charge (0.82).

The nearest distance from the metal atom to the carbon atom (M–C distance) is also shown in Table 2. The M–C distances of the second-row metal atoms are shorter than those of the third-row metal atoms. This reflects the size of the metal atom. The lower limit of the atom size is given by its ionic radius. The ionic radii of Li^+, Na^+, Be^{2+}, and Mg^{2+} derived from crystallographic data are 0.73, 1.13, 0.41, and 0.71 Å, respectively [33]. Subtracting the ionic radius from the M–C distance yields the radius of the adjacent carbon atom. The calculated carbon radii of structures **7**, **9**, **11**, and **12** (1.42 to 1.49 Å) are close to the radius of carbon monoanion (1.48 Å) determined by the minimum of the electrostatic static potential [34]. Structures **8** and **10**, which contain Li dimmers, show small carbon radii (1.33 to 1.34 Å) reflecting the covalent character of their Li–C bonds. A small carbon radius is also found in structure **13** (1.34 Å). Structure **14** shows a large carbon radius (1.62 Å) comparable to its van der Waals radius (1.70 Å). This overestimation is caused by subtracting the small Mg^{2+} radius from the Mg–C distance. The small charge of the Mg atom in **14** indicates that the Mg atom is not fully ionized and has a larger radius than Mg^{2+}.

3.3 Hydrogen adsorption on Li, Na, Be, and Mg atoms attached to aromatic hydrocarbons

Hydrogen adsorption on metal atoms attached to the hydrocarbons was examined by adding one hydrogen molecule on the metal atom. Structures **7**, **9**, **11**, and **12** have two different adsorption sites, and thus 12 structures were examined in total. Optimized structures of $Li_2C_6H_6$-H_2 (**15**–**17**), $Li_2C_{14}H_{10}$-H_2 (**18**–**20**), $Na_2C_{14}H_{10}$-H_2 (**21**–**24**), $BeC_{14}H_{10}$-H_2 (**25**), and $MgC_{14}H_{10}$-H_2 (**26**) are shown in Fig. 3. Structures **15**–**26** were optimized adopting no symmetry. Obtained structures seem to have C_s symmetry except **15** and **16**. The binding energy of a hydrogen molecule is shown in Table 3 with the change in H–H bond length from its equilibrium distance (0.737 Å) and the NPA charge of the H_2 molecule.

The hydrogen binding energies of the structures other than **25** are in the range of −4.0 to −0.3 kcal/mol. These structures show small changes in the H–H bond length (0.003 to 0.01 Å) and in the H_2 charge (0.001 to 0.15). These results indicate that their hydrogen binding mechanism is physisorption. On the other hand, structure **25**, where the H_2

Table 3 Binding energy of a hydrogen molecule adsorbed on a metal atom attached to hydrocarbon molecules (ΔE_{H_2}), the change in H–H bond length (ΔR_{H_2}), the H_2 charge (q_{H_2}), the distance between the center of mass of the H_2 molecule and the metal atom (R_{M-H_2}), and the distance between the center of mass of the H_2 molecule and that of the C_6-ring ($R_{C_6-H_2}$). The energy without CP correction is shown in parentheses. The calculated bond length of an isolated H_2 molecule is 0.737 Å

	ΔE_{H_2}/kcal mol^{-1}	ΔR_{H_2}/Å	q_{H_2}	R_{M-H_2}/Å	$R_{C_6-H_2}$/Å
$Li_2C_6H_6$-H_2					
15	−2.6(−2.9)	+0.007	+0.005	2.03	3.74
16	−2.2(−2.6)	+0.009	+0.001	2.05	3.51
17	−2.7(−3.0)	+0.007	+0.006	2.01	4.04
$Li_2C_{14}H_{10}$-H_2					
18	−4.0(−4.4)	+0.010	+0.012	2.05	2.89
19	−3.1(−3.5)	+0.007	+0.010	2.01	3.67
20	−3.9(−4.4)	+0.009	+0.015	2.02	2.88
$Na_2C_{14}H_{10}$-H_2					
21	−2.8(−3.3)	+0.008	+0.001	2.52	2.77
22	−2.1(−2.4)	+0.007	−0.006	2.47	3.67
23	−1.8(−2.2)	+0.007	+0.001	2.46	2.94
24	−0.3(−0.4)	+0.003	+0.003	2.79	4.13
$BeC_{14}H_{10}$-H_2					
25	−8.6(−9.4)	+0.033	+0.033	1.58	2.96
$MgC_{14}H_{10}$-H_2					
26	−1.3(−1.8)	+0.008	+0.002	2.75	3.12

molecule is bound on the Be atom, shows much more negative binding energy (−8.6 kcal/mol) than the others, with larger changes in the H–H bond length (0.033 Å) and the H_2 charge (0.033). These characteristics indicate that the binding mechanism of **25** involves a charge transfer process from the H_2 molecule, which should be distinguished from the pure physisorption.

Among the physisorbed structures, $Li_2C_{14}H_{10}$-H_2 complexes show more negative binding energies (−4.0 to −3.1 kcal/mol) than the others. These energies are comparable to the minimal energy (−3.6 kcal/mol) for a hydrogen storage/release at ambient temperature with moderate pressure [2, 35]. These complexes have large positive Li charges as shown in the previous section. Table 3 shows the distance between the metal atom and the center of mass of the H_2 molecules (M–H_2 distance). Li–H_2 distances (2.01 to 2.05 Å) are shorter than the Na–H_2 and Mg–H_2 distances (2.47 to 2.79 Å) owing to the size of metal atoms. These observations suggest that the hydrogen binding energy becomes more negative as the metal atom has more positive charge and a smaller radius.

To test the level of theory and the size of the basis set, we additionally calculated the MP2 and MP3 binding energies of a H_2 molecule on a CH_3Li molecule using the optimized structure at MP2/cc-pVTZ level where the Li atomic charge was +0.818. The MP2 (MP3) binding energy with CP correction was 1.98 (2.03) kcal/mol and its CBS limit was 2.10 (2.14) kcal/mol. These results show that the CBS limit does not much influence the magnitude of the binding energy and the MP3 method gives almost the same energy as the MP2 method.

The positive charge of metal atom attached to the hydrocarbon can polarize a hydrogen molecule and induce a dipole on it. This dipole interacts with the metal atom, and the induction force comes to act between them as an attractive force. Assuming that the metal atom is represented by a point charge and the H_2 molecule has spherical shape, the induction energy is written as

$$U_{\mathrm{Ind}}(R_{M-H_2}) = -\frac{1}{2}\frac{q_M^2 \alpha_{H_2}}{R_{M-H_2}^4}, \tag{2}$$

where q_M, α_{H_2}, and R_{M-H_2} denote the charge of the metal atom, the polarizability of the H_2 molecule, and the M–H_2 distance, respectively. Using the averaged polarizability (3.9 Bohr^3) for α_{H_2}, the induction energy was calculated for structures **15**–**26**. Results are shown in Table 4. In Fig. 4, the induction energies are plotted against the ab initio hydrogen binding energies. The induction energy of **25** is not plotted because it deviates greatly from the ab initio result. The induction energy has almost the same magnitude as the ab initio energy and tends to increase in proportion to it. This means that the induction energy is one of the major components of the hydrogen binding energy.

However, some data deviate greatly from the diagonal line in Fig. 4. For example, the point for structure **19** is located far below and those for structures **21** and **23** are located far above the diagonal line. The induction energy overestimates the attraction for points below the diagonal line, while it underestimates for those above the diagonal line. To correct these deviations, the former points require repulsive and the latter points require another attractive force.

Table 4 Components of the binding energy of a hydrogen molecule adsorbed on the metal atom attached to hydrocarbons: the induction potential (U_{Ind}), the minimum energy of the induction potential with repulsion ($U_{\mathrm{M}}^{\mathrm{min}}$), and the minimum energy of the Lennard–Jones potential between the H_2 molecule and the nearest C_6-ring ($U_{\mathrm{L\text{–}J}}^{\mathrm{min}}$). The unit is kcal/mol

	U_{Ind}	$U_{\mathrm{M}}^{\mathrm{min}}$	$U_{\mathrm{L\text{–}J}}^{\mathrm{min}}$		$\Delta E_{\mathrm{H_2}} - (U_{\mathrm{M}}^{\mathrm{min}} + U_{\mathrm{L\text{–}J}}^{\mathrm{min}})$	
			$B = B_{\mathrm{av}}$	$A = A_{\mathrm{av}}$	$B = B_{\mathrm{av}}$	$A = A_{\mathrm{av}}$
$Li_2C_6H_6$-H_2						
15	−3.0	−2.0	−0.2	−0.1	−0.4	−0.5
16	−2.9	−1.9	−0.3	−0.1	−0.0	−0.2
17	−3.2	−2.1	−0.1	−0.0	−0.5	−0.6
$Li_2C_{14}H_{10}$-H_2						
18	−4.0	−2.6	−1.1	−1.2	−0.3	−0.1
19	−4.9	−3.3	−0.3	−0.1	0.4	0.2
20	−3.5	−2.3	−1.1	−1.3	−0.5	−0.4
$Na_2C_{14}H_{10}$-H_2						
21	−1.2	−0.8	−1.4	−2.0	−0.7	−0.0
22	−2.0	−1.3	−0.3	−0.1	−0.5	−0.7
23	−0.9	−0.6	−1.0	−1.0	−0.3	−0.3
24	−0.6	−0.4	−0.1	−0.0	0.2	0.1
$BeC_{14}H_{10}$-H_2						
25	−26.2	−17.5	−0.9	−0.9	9.8	9.8
$MgC_{14}H_{10}$-H_2						
26	−1.1	−0.7	−0.7	−0.5	0.1	−0.1

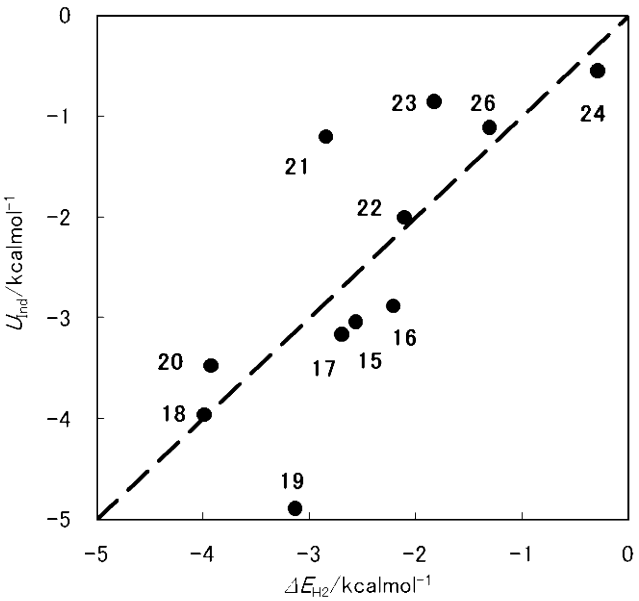

Fig. 4 Induction energy plotted against the hydrogen binding energy with CP correction

To correct the overestimation of the attraction, a repulsive term proportional to $R_{\mathrm{M\text{–}H_2}}^{-12}$ is added to the induction energy. Then the potential energy of the H_2 molecule adsorbed on the metal atom is given as

$$U_{\mathrm{M}}(R_{\mathrm{M\text{–}H_2}}) = \frac{C}{R_{\mathrm{M\text{–}H_2}}^{12}} - \frac{1}{2}\frac{q_{\mathrm{M}}^2 \alpha_{\mathrm{H_2}}}{R_{\mathrm{M\text{–}H_2}}^4}. \tag{3}$$

The coefficient C can be determined by the relation

$$C = \frac{1}{6} q_{\mathrm{M}}^2 \alpha_{\mathrm{H_2}} {R_{\mathrm{M\text{–}H_2}}^{\mathrm{eq}}}^4, \tag{4}$$

where $R_{\mathrm{M\text{–}H_2}}^{\mathrm{eq}}$ denotes the equilibrium M–H_2 distance. Then the minimum of U_{M} is given as

$$U_{\mathrm{M}}(R_{\mathrm{M\text{–}H_2}}^{\mathrm{eq}}) = \frac{2}{3} U_{\mathrm{Ind}}(R_{\mathrm{M\text{–}H_2}}^{\mathrm{eq}}). \tag{5}$$

Regarding the M–H_2 distance in Table 3 as the equilibrium distance, the minimum of U_{M} ($U_{\mathrm{M}}^{\mathrm{min}}$) was estimated for each structure; the results are shown in Table 4.

In Fig. 5, the $U_{\mathrm{M}}^{\mathrm{min}}$ energies are plotted against the ab initio energies. Although the deviations caused by the overestimation of the attraction are corrected, addition of the repulsive term makes most of the points appear above the diagonal line. In particular, the points for structures **18**, **20**, **21**, and **23** deviate greatly from the diagonal line by 1.3 to 2.0 kcal/mol. Thus, another attraction other than induction works in these structures.

In Table 3, the distance between the center of mass of the H_2 molecule and that of the nearest C_6-ring is shown for structures **15**–**26**. The C_6–H_2 distances of **18**, **20**, **21**, and **23** are shorter (2.77 to 2.94 Å) than the others (3.12 to 4.13 Å) and they are comparable to those of H_2–anthracene complexes **4**–**6** (2.88 to 3.00 Å). Therefore, the dispersion force between the H_2 molecule and the C_6-ring is expected to contribute considerably to the hydrogen binding energy for these structures.

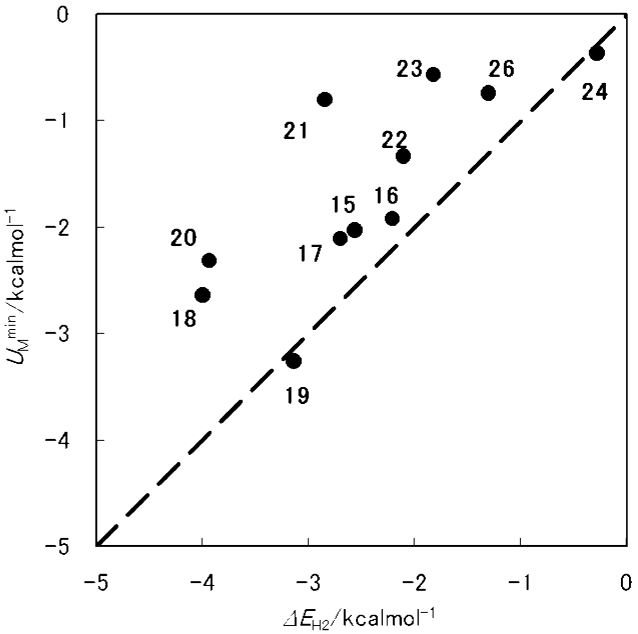

Fig. 5 The minimum of the induction energy with repulsion plotted against the hydrogen binding energy with CP correction

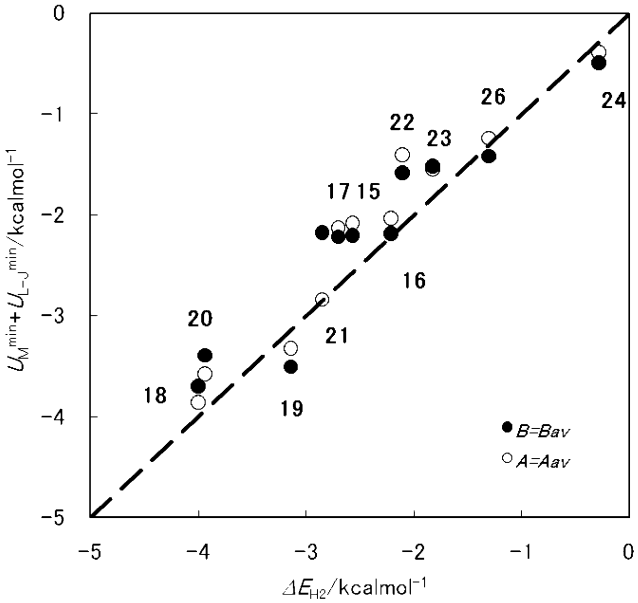

Fig. 6 The sum of the minimum of the induction energy with repulsion and minimum of the Lennard–Jones potential energy plotted against the hydrogen binding energy with CP correction. The open (filled) circles represent the energy calculated using the averaged parameter A_{av} (B_{av})

To evaluate this dispersion force for structures **15**–**26**, the Lennard–Jones potential given by (1) is used. Because the A and B parameters of the potential are unknown for these structures, they are determined in the following manner. Assuming that the parameters of the structures **15**–**17** (**18**–**26**) have values close to those of **1**–**3** (**4**–**6**), either of the parameters is approximated by the coefficient averaged over structures **1**–**3** (**4**–**6**). The other coefficient is determined by the relation

$$\frac{A}{B} = \frac{1}{2} {R^{eq}_{C_6-H_2}}^6, \tag{6}$$

where $R^{eq}_{C_6-H_2}$ denotes the equilibrium C_6–H_2 distance. Regarding the C_6–H_2 distance in Table 3 as the equilibrium distance, the minimum of U_{L-J} (U^{min}_{L-J}) was estimated.

The values of U^{min}_{L-J} calculated by using A_{av} and B_{av}, respectively, are shown in Table 4. The difference between these two energies is about ±0.2 kcal/mol for each structure except **21**. For **21**, the use of A_{av} gives a more negative U^{min}_{L-J} than the use of B_{av} by −0.6 kcal/mol. The sum of U^{min}_{L-J} and U^{min}_{M} gives an approximate energy of ΔE_{H_2}. The difference between ΔE_{H_2} and $U^{min}_{M} + U^{min}_{L-J}$ is also shown in Table 4. It is observed that the use of A_{av} gives a closer energy than the use of B_{av} for structures having an $R_{C_6-H_2}$ smaller than 3.0 Å (group **I**) except **25**. The value of U^{min}_{L-J} in group **I** is in the range of −2.0 to −1.0 kcal/mol. On the other hand, the use of B_{av} gives a closer energy than the use of A_{av} for those having an $R_{C_6-H_2}$ larger than 3.0 Å (group **II**) except **19** and **24**. Because U^{min}_{M} is already more negative than ΔE_{H_2} by −0.3 to −0.1 kcal/mol for **19** and **24**, a more negative U^{min}_{L-J} gives a larger deviation from ΔE_{H_2}. To correct these deviations, a more repulsive term than $R^{-12}_{M-H_2}$ should be incorporated into U_M. The value of U^{min}_{L-J} in group **II** is in the range of −0.7 to −0.1 kcal/mol. From these observations, it may be presumed that the structures in group **I** have more negative attractive potentials than the H_2–hydrocarbon complexes, while those in group **II** have more positive repulsive potentials.

In Fig. 6, the sum of U^{min}_{M} and U^{min}_{L-J} is plotted against ΔE_{H_2}. The points for **18**, **20**, **21**, and **23**, which showed large deviations in Fig. 5, have come close to the diagonal line. The other points are also located near this line. It is recognized that the sum of U^{min}_{M} and U^{min}_{L-J} gives a good approximation to ΔE_{H_2}.

The sum of U^{min}_{M} and U^{min}_{L-J} dominates more than 76% of ΔE_{H_2}. The main component of ΔE_{H_2} is the U^{min}_{M} for structures in group **II**, including **19** and **24**. The U^{min}_{M} comprises more than 62% and the U^{min}_{L-J} less than 14% of ΔE_{H_2}. On the other hand, the main component alternates between Li- and Na-attached anthracene molecules for structures in group **I**. The U^{min}_{M} occupies 59 to 65% and U^{min}_{L-J} occupies 30 to 37% of ΔE_{H_2} for the Li-attached anthracene molecules (**18** and **20**), whereas the U^{min}_{M} occupies 29 to 33% and U^{min}_{L-J} occupies 56 to 71% of ΔE_{H_2} for the Na-attached anthracene molecules (**21** and **23**). It is noticeable that the contributions of U^{min}_{L-J} are not negligible for structures **18** and **20**, which show more negative ΔE_{H_2} than the others.

4 Conclusions

It has been shown that the hydrogen binding energy on Li, Na, and Mg atoms attached to the aromatic hydrocarbon molecules (benzene and anthracene) mainly consisted of the induction force caused by the positive charge of the metal atom and the dispersion force from the nearest C_6-ring. Among them some Li-attached anthracene molecules show more negative hydrogen binding energies (−4.0 to −3.9 kcal/mol) than the others (−3.1 to −0.3 kcal/mol) because their Li atoms have more positive charges and smaller radii than the other atoms, and they can effectively utilize the dispersion force from the C_6-ring neighboring the hydrogen molecule. The energies are comparable to the minimal energy (−3.6 kcal/mol) to operate hydrogen storage/release at ambient temperature with moderate pressure.

The contribution of the zero-point vibrational energy (ZPE) to the hydrogen binding energy was not elucidated in this study. The ZPE cannot be ignored for the weak binding treated in this study. However, the exact calculation of the ZPE with regard to the intermolecular interaction is very difficult because of the vibrational anharmonicity inherent to it [31].

Finally, setting aside the toxicity of Be, it should be pointed out that the hydrogen binding on the Be atom, which involves charge transfer from the H_2 molecule to the Be atom, shows the most negative energy (−8.6 kcal/mol) among the investigated metal atoms.

Acknowledgements This study was performed as part of the Project of the Academic Frontier Center at the Nagasaki Institute of Applied Science and was partly supported by a Grant-in-Aid for Scientific Research from the Japan Society for the Promotion of Science (JSPS-17350094 and JSPS-20350089).

References

1. Hydrogen Fuel Cells and Infrastructure Technologies Programs, US Department of Energy (http://www.eere.energy.gov/hydrogenandfuelcells/about.html) (2009)
2. A.W.C. van den Berg, C.O. Areán, Chem. Commun. 668 (2008)
3. F.L. Darklim, P. Malbrunot, G.P. Tartaglia, Int. J. Hydrog. Energy **27**, 193 (2002)
4. M. Hirscher, M. Becher, M. Haluska, U. Dettlaff-Weglikowska, A. Quintel, G.S. Duesberg, P. Downes, Y.-M. Choi, M. Hulman, S. Roth, I. Stepanek, P. Bernier, Appl. Phys. A **72**, 129 (2001)
5. R. Yang, Carbon **38**, 623 (2000)
6. E. Poirier, R. Chahine, P. Bénard, D. Cossement, L. Lafi, E. Mélançon, T.K. Bose, S. Désilets, Appl. Phys. A **78**, 961 (2004)
7. B. Panella, M. Hirscher, S. Roth, Carbon **43**, 2209 (2005)
8. R. Dash, J. Chmiola, G. Yushin, Y. Gogosti, G. Landisio, J. Singer, J. Fischer, S. Kucheyev, Carbon **44**, 2489 (2006)
9. M. Shiraishi, T. Takenobu, H. Katakura, M. Ata, Appl. Phys. A **78**, 947 (2004)
10. B. Panella, M. Hirscher, B. Ludesdcher, Microporous Mesoporous Mater. **103**, 230 (2007)
11. L. Mattera, F. Rosatelli, C. Salvo, F. Tommasini, U. Valbusa, G. Vidali, Surf. Sci. **93**, 515 (1980)
12. G. Vidali, G. Ihm, H.-Y. Kim, M.W. Cole, Surf. Sci. Rep. **12**, 133 (1991)
13. P. Kowalczyk, R. Hołsyt, M. Terrones, H. Terrones, Phys. Chem. Chem. Phys. **9**, 1786 (2007)
14. M. Bonfanti, R. Martinazzo, G.F. Tantardini, A. Ponti, J. Phys. Chem. C **111**, 5825 (2007)
15. S.S. Han, J.K. Kang, H.M. Lee, A.C.T. van Duin, W.A. Goddard III, Appl. Phys. Lett. **86**, 203108 (2005)
16. A.C.T. van Duin, S. Dasgupta, F. Lorant, W.A. Goddard III, J. Phys. Chem. A **105**, 9396 (2001)
17. M.J. Frisch, G.W. Trucks, H.B. Schlegel, G.E. Scuseria, M.A. Robb, J.R. Cheeseman, J.A. Montgomery Jr., T. Vreven, K.N. Kudin, J.C. Burant, J.M. Millam, S.S. Iyengar, J. Tomasi, V. Barone, B. Mennucci, M. Cossi, G. Scalmani, N. Rega, G.A. Petersson, H. Nakatsuji, M. Hada, M. Ehara, K. Toyota, R. Fukuda, J. Hasegawa, M. Ishida, T. Nakajima, Y. Honda, O. Kitao, H. Nakai, M. Klene, X. Li, J.E. Knox, H.P. Hratchian, J.B. Cross, V. Bakken, C. Adamo, J. Jaramillo, R. Gomperts, R.E. Stratmann, O. Yazyev, A.J. Austin, R. Cammi, C. Pomelli, J.W. Ochterski, P.Y. Ayala, K. Morokuma, G.A. Voth, P. Salvador, J.J. Dannenberg, V.G. Zakrzewski, S. Dapprich, A.D. Daniels, M.C. Strain, O. Farkas, D.K. Malick, A.D. Rabuck, K. Raghavachari, J.B. Foresman, J.V. Ortiz, Q. Cui, A.G. Baboul, S. Clifford, J. Cioslowski, B.B. Stefanov, G. Liu, A. Liashenko, P. Piskorz, I. Komaromi, R.L. Martin, D.J. Fox, T. Keith, M.A. Al-Laham, C.Y. Peng, A. Nanayakkara, M. Challacombe, P.M.W. Gill, B. Johnson, W. Chen, M.W. Wong, C. Gonzalez, J.A. Pople, *Gaussian 03, Revision B.04* (Gaussian, Inc., Wallingford, 2004)
18. C. Möller, M.S. Plesset, Phys. Rev. **46**, 618 (1934)
19. D.E. Woon, T.H. Dunning Jr, J. Chem. Phys. **98**, 1358 (1993)
20. S.F. Boys, F. Bernardi, Mol. Phys. **19**, 553 (1970)
21. S. Simon, M. Duran, J.J. Dannenberg, J. Chem. Phys. **105**, 11024 (1996)
22. A.E. Reed, R.B. Weinstock, F. Weinhold, J. Chem. Phys. **83**, 735 (1985)
23. N.C. Handy, H.F. Schaefer III, J. Chem. Phys. **81**, 5031 (1984)
24. F. Tran, J. Weber, T.A. Wesolowski, F. Cheikh, Y. Ellinger, F. Pauzat, J. Phys. Chem. B **106**, 8689 (2002)
25. O. Hübner, A. Glöss, M. Fichtner, W. Klopper, J. Phys. Chem. A **108**, 3019 (2004)
26. H. Krause, B. Ernstberger, H.J. Neusser, Chem. Phys. Lett. **184**, 411 (1991)
27. J.R. Grover, E.A. Walters, E.T. Hui, J. Chem. Phys. **91**, 3233 (1987)
28. M.O. Sinnokrot, E.F. Valeev, C.D. Sherrill, J. Am. Chem. Soc. **124**, 10887 (2002)
29. M.O. Sinnokrot, C.D. Sherrill, J. Phys. Chem. A **110**, 10656 (2006)
30. T. Janowski, P. Pulay, Chem. Phys. Lett. **447**, 27 (2007)
31. M.W. Feyereisen, D. Feller, D.A. Dixson, J. Phys. Chem. **100**, 2993 (1996)
32. S. Ishikawa, G. Madjarova, T. Yamabe, J. Phys. Chem. B **105**, 11986 (2001)
33. R.D. Shannon, Acta Crystallogr. Sect. A **32**, 751 (1969)
34. K.D. Sen, P. Politzer, J. Chem. Phys. **90**, 4370 (1989)
35. S.R. Bhatia, A.L. Myers, Langmuir **22**, 1688 (2006)